



HAL
open science

Intrinsic and photo-induced properties of high refractive index azobenzene based thin films [Invited]

E. Mavrona, S. Mailis, N. Podoliak, G. d'Alessandro, N. Tabiryan, M. Trapatseli, Jean-François Blach, M. Kaczmarek, V. Apostolopoulos

► **To cite this version:**

E. Mavrona, S. Mailis, N. Podoliak, G. d'Alessandro, N. Tabiryan, et al.. Intrinsic and photo-induced properties of high refractive index azobenzene based thin films [Invited]. *Optical Materials Express*, 2018, 8 (2), pp.420-430. 10.1364/OME.8.000420 . hal-01691569

HAL Id: hal-01691569

<https://hal.science/hal-01691569>

Submitted on 20 Nov 2023

HAL is a multi-disciplinary open access archive for the deposit and dissemination of scientific research documents, whether they are published or not. The documents may come from teaching and research institutions in France or abroad, or from public or private research centers.

L'archive ouverte pluridisciplinaire **HAL**, est destinée au dépôt et à la diffusion de documents scientifiques de niveau recherche, publiés ou non, émanant des établissements d'enseignement et de recherche français ou étrangers, des laboratoires publics ou privés.



Intrinsic and photo-induced properties of high refractive index azobenzene based thin films [Invited]

E. MAVRONA,^{1,2,3} S. MAILIS,⁴ N. PODOLIAK,¹ G. D'ALESSANDRO,⁵
N. TABIRYAN,⁶ M. TRAPATSELI,⁷ J.-F. BLACH,² M. KACZMAREK,^{1,*}
AND V. APOSTOLOPOULOS¹

¹Physics and Astronomy, University of Southampton, Southampton SO17 1BJ, UK

²Univ. Artois, CNRS, Centrale Lille, ENSCL, Univ. Lille, UMR 8181, Unité de Catalyse et de Chimie du Solide (UCCS), F-62300 Lens, France

³Institute of Quantum Electronics Quantum Optoelectronics Group, ETH Zurich, Auguste-Piccard-Hof 1, 8093 Zurich, Switzerland

⁴Optoelectronics Research Centre, University of Southampton, Southampton SO17 1BJ, UK

⁵Mathematical Sciences, University of Southampton, Southampton SO17 1BJ, UK

⁶Beam Engineering for Advanced Measurements Company, 809 South Orlando Avenue Suite I, Winter Park, FL 32789, USA

⁷Electronics and Computer Science, University of Southampton, Southampton SO17 1BJ, UK

*mfk@soton.ac.uk

Abstract: We explore the limits of the photosensitive response of thin, 15 to 35 nm, films of complex azobenzene dyes. They show high refractive index, reaching 1.8, and significant photo-induced birefringence. We have successfully recorded strong, birefringent phase gratings with visible light and used the diffraction efficiency measurements to monitor their temporal evolution. The photo-induced gratings in such thin films were found not to be associated with any periodic surface relief, a typical feature in thicker azobenzene layers.

Published by The Optical Society under the terms of the [Creative Commons Attribution 4.0 License](#). Further distribution of this work must maintain attribution to the author(s) and the published article's title, journal citation, and DOI.

OCIS codes: (160.5335) Photosensitive materials; (160.4760) Optical properties; (160.3710) Liquid crystals; (160.1190) Anisotropic optical materials; (310.5448) Polarization, other optical properties; (050.1950) Diffraction gratings.

References and links

1. A. Priimagi and A. Shevchenko, "Azopolymer-based micro- and nanopatterning for photonic applications," *J. Polym. Sci. Part B: Polym. Phys.* **52**, 163–182 (2014).
2. J. Griffiths, "Photochemistry of azobenzene and its derivatives," *Chem. Soc. Rev.* **1**, 481–493 (1972).
3. F. P. Nicoletta, D. Cupelli, P. Formoso, G. De Filpo, V. Colella, and A. Gugliuzza, "Light responsive polymer membranes: A review," *Membranes* **2**, 134–197 (2012).
4. G. S. Kumar and D. C. Neckers, "Photochemistry of azobenzene-containing polymers," *Chem. Rev.* **89**, 1915–1925 (1989).
5. S. Hosotte and M. Dumont, "Orientational relaxation of photomerocyanine molecules in polymeric films," *Synth. Met.* **81**, 125–127 (1996).
6. J. Kauppo, "Photoalignment control and surface-relief gratings in commercial azobenzene-based photoalignment layers," Bachelor's thesis thesis supervisor: Prof. Matti Kaivola thesis advisor: D.Sc. (Tech.) Arri Priimagi, School of Science, Aalto University (2014).
7. M. L. Dumont, S. Hosotte, G. Froc, and Z. Sekkat, "Orientational manipulation of chromophores through photoisomerization," in "Photopolymers and Applications in Holography, Optical Data Storage, Optical Sensors, and Interconnects," R. A. Lessard, ed. (SPIE-Intl Soc Optical Eng, 1994).
8. L. Frey, M. Kaczmarek, J. M. Jonathan, and G. Roosen, "Analysis of gratings induced in azo-dye doped liquid crystals," *Opt. Mat.* **18**, 91–94 (2001).
9. S. R. Nersisyan, N. V. Tabiryan, D. M. Steeves, B. R. Kimball, V. G. Chigrinov, and H. S. Kwok, "Study of azo dye surface command photoalignment material for photonics applications," *Appl. Opt.* **49**, 1720–1727 (2010).
10. L. De Sio, G. Klein, S. Serak, N. Tabiryan, A. Cunningham, C. M. Tone, F. Ciuchi, T. Burgi, C. Umeton, and T. Bunning, "All-optical control of localized plasmonic resonance realized by photoalignment of liquid crystals," *J. Mater. Chem. C* **1**, 7483–7487 (2013).

11. S. Nersisyan, N. Tabiryan, D. M. Steeves, and B. R. Kimball, "Axial polarizers based on dichroic liquid crystals," *J. Appl. Phys.* **108**, 033101 (2010).
 12. G. Pawlik, A. C. Mitus, J. Mysliwiec, A. Miniewicz, and J. G. Grote, "Photochromic dye semi-intercalation into dna-based polymeric matrix: Computer modeling and experiment," *Chemical Physics Letters* **484**, 321–323 (2010).
 13. F. Lagugné Labarthe, T. Buffeteau, and C. Sourisseau, "Analyses of the diffraction efficiencies, birefringence, and surface relief gratings on azobenzene-containing polymer films," *J. Phys. Chem. B* **102**, 2654–2662 (1998).
 14. J. Gao, Y. He, F. Liu, X. Zhang, Z. Wang, and X. Wang, "Azobenzene-containing supramolecular side-chain polymer films for laser-induced surface relief gratings," *Chem. Mater.* **19**, 3877–3881 (2007).
 15. O. R. Bennani, T. A. Al-Hujran, J.-M. Nunzi, R. G. Sabat, and O. Lebel, "Surface relief grating growth in thin films of mexylaminotriazine-functionalized glass-forming azobenzene derivatives," *New J. Chem.* **39**, 9162–9170 (2015).
 16. F. Lagugné Labarthe, T. Buffeteau, and C. Sourisseau, "Azopolymer holographic diffraction gratings: time dependent analyses of the diffraction efficiency, birefringence, and surface modulation induced by two linearly polarized interfering beams," *J. Phys. Chem. B* **103**, 6690–6699 (1999).
 17. F. Lagugné Labarthe, P. Rochon, and A. Natansohn, "Polarization analysis of diffracted orders from a birefringence grating recorded on azobenzene containing polymer," *Appl. Phys. Lett.* **75**, 1377–1379 (1999).
 18. M. Watabe, G. Juman, K. Miyamoto, and T. Omatu, "Light induced conch-shaped relief in an azo-polymer film," *Sci. Rep.* **4**, 1–4 (2014).
 19. N. Tsutsumi, "Recent advances in photorefractive and photoactive polymers for holographic applications," *Polym. Int.* **66**, 167–174 (2017).
 20. F. You, M. Y. Paik, M. Häckel, L. Kador, D. Kropp, H. W. Schmidt, and C. K. Ober, "Control and suppression of surface relief gratings in liquid-crystalline perfluoroalkyl-azobenzene polymers," *Adv. Funct. Mater.* **16**, 1577–1581 (2006).
 21. L. Miccio, M. Paturzo, A. Finizio, and P. Ferraro, "Light induced patterning of poly(dimethylsiloxane) microstructures," *Opt. Exp.* **18**, 10947–10955 (2010).
 22. A. Priimagi, J. Vapaavuori, F. J. Rodriguez, C. F. J. Faul, M. T. Heino, O. Ikkala, M. Kauranen, and M. Kaivola, "Hydrogen-bonded polymer–azobenzene complexes: Enhanced photoinduced birefringence with high temporal stability through interplay of intermolecular interactions," *Chem. Mater.* **20**, 6358–6363 (2008).
 23. Q. Guo, A. Srivastava, V. Chigrinov, and H. Kwok, "Polymer and azo-dye composite: a photo-alignment layer for liquid crystals," *Liq. Cryst.* **41**, 1465–1472 (2014).
 24. O. Yaroshchuk and Y. A. Reznikov, "Photoalignment of liquid crystals: basics and current trends," *J. Mater. Chem.* **22**, 286–300 (2012).
 25. K. L. Marshall, O. Didovets, and D. Saulnier, "Contact-angle measurements as a means of probing the surface alignment characteristics of liquid crystal materials on photoalignment layers," in "Liquid Crystals XVIII," I. C. Khoo, ed. (SPIE, 2014).
 26. S. Serak, T. Bunning, and N. Tabiryan, "Ultrafast photoalignment: Recording a lens in a nanosecond," *Crystals* **7**, 338 (2017).
 27. M. Bouzige, P. Legeay, V. Pichon, and M.-C. Hennion, "Selective on-line immunoelectroextraction coupled to liquid chromatography for the trace determination of benzidine, congeners and related azo dyes in surface water and industrial effluents," *J. Chromatogr. A* **846**, 317 – 329 (1999).
 28. E. A. Harland G. Tompkins, Irene, ed., *Handbook of ellipsometry* (William Andrew, Inc, 2005).
 29. J. N. Hilfiker, N. Singh, T. Tiwald, D. Convey, S. M. Smith, J. H. Baker, and H. G. Tompkins, "Survey of methods to characterize thin absorbing films with spectroscopic ellipsometry," *Thin Solid Films* **516**, 7979 – 7989 (2008). Proceedings of the EMRS 2007 Fall Meeting Symposium H: Current trends in optical and x-ray metrology of advanced materials and devices {II} Warsaw, Poland.
 30. Y. J. Ying, C. E. Valdivia, C. L. Sones, R. W. Eason, and S. Mailis, "Latent light-assisted poling of LiNbO₃," *Opt. Exp.* **17**, 18681–18692 (2009).
 31. M. Trapatseli, D. Carta, A. Regoutz, A. Khat, A. Serb, I. Gupta, and T. Prodromakis, "Conductive atomic force microscopy investigation of switching thresholds in titanium dioxide thin films," *J. Phys. Chem* **119**, 11958–11964 (2015).
 32. J. W. Weber, T. A. R. Hansen, M. C. M. van de Sanden, and R. Engeln, "B-spline parametrization of the dielectric function applied to spectroscopic ellipsometry on amorphous carbon," *J. Appl. Phys.* **106**, 123503 (2009).
 33. G. Jellison, "Data analysis for spectroscopic ellipsometry," *Thin Solid Films* **234**, 416 – 422 (1993).
 34. O. M. Tanchak, , and C. J. Barrett, "Light-induced reversible volume changes in thin films of azo polymers: The photomechanical effect," *Macromolecules* **38**, 10566–10570 (2005).
 35. C. Raman and N. N. Nath, "The diffraction of light by high frequency sound waves, part 1," *Proc. Indian Acad. Sci.* **2**, 406–412 (1935).
 36. C. Raman and N. N. Nath, "The diffraction of light by high frequency sound waves, part 2," *Proc. Indian Acad. Sci.* **2**, 413–420 (1935).
 37. R. Magnusson and T. K. Gaylord, "Diffraction efficiencies of thin phase gratings with arbitrary grating shape," *J. Opt. Soc. Am.* **68**, 806 (1978).
-

1. Introduction

Azobenzene based materials exhibit strong, selective photosensitivity and have been explored for different photonic applications [1]. They undergo photo-chemical isomerization from the *trans* form to the less stable *cis* form, under irradiation with UV and visible light [2] to achieve a photo-stationary composition that is wavelength and temperature dependent. The photo-chemical or thermal isomerism between the *cis* and *trans* forms [1, 3] is shown in Fig. 1. The *trans*-isomer preferentially absorbs UV and blue photons polarized parallel to its molecular axis, changing the conformation of the $N=N$ bond at the center of the molecule. As such the isomer transforms into its *cis* form. The *cis* isomer is shorter than the *trans* isomer [4] (0.6 nm against 1 nm), has different dipole moment and, hence, refractive index. The lifetime of the *cis* state is molecule dependent [5], but it is, in general, relatively short lived [6] (~ 1 s) in the case of interest for liquid crystal alignment. The *cis* isomer decays back to the *trans*- isomer with a random orientation (Angular Hole Burning model [7]). Therefore, the net effect of prolonged illumination of an azo-based layer is the preferential alignment of its molecules in the direction perpendicular to the incident light local polarization, which has also been explored for writing gratings in guest-host liquid crystal systems [8]. This orientation process is reversible [9], but stable in ambient conditions. Such azobenzene layers can optically encode high resolution patterns, which are used as polarization gratings and spiral phase wave-plates [10–12].

When illuminated by the interference pattern of two laser beams, thick azo-based layers (100 nm to 2 μm) form surface relief gratings [13–15] (SRGs), with troughs as deep as 200–300 nm. Their depth depends on the polarization and intensity of the recording laser beams, and on the recording duration [16]. In particular, while circularly polarized beams can produce relatively deep surface reliefs also in the thinner layers considered in these studies (thickness ~ 150 nm), linearly polarized beams produce a very shallow relief [17]. More complex surface relief patterns were also demonstrated using, for example, incident vortex beams [18].

In liquid crystal display applications, much thinner layers, with thicknesses of the order of a few tens of nanometers, are used. They have been mostly considered for their effect on the neighboring materials, in particular for photo-aligning liquid crystals [10, 11, 19–24]. In relevant studies the main focus was on their strong influence in modulating liquid crystal orientation and the associated applications for waveplates. However, despite extensive investigations of very thin films of azo-based materials for liquid crystal photo-alignment, there is little information on their intrinsic optical properties.

In this work, we investigated thin layers (up to 35 nm) of azo-benzene materials, namely PAAD complex azo-dyes [11], as *stand alone* films not integrated with other materials, to characterize their optical properties and investigate any photo-induced response. In particular,

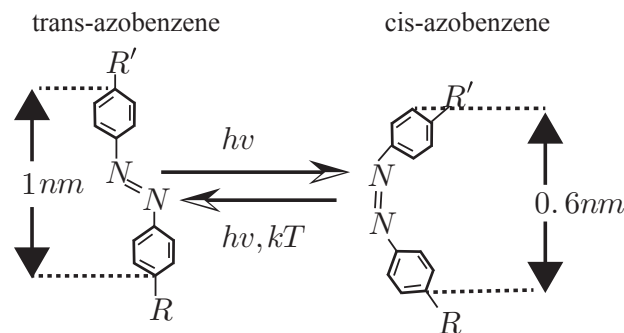


Fig. 1. Schematic representation of the photo-chemical isomerization between *trans*- and *cis*- forms in azobenzene based materials [3].

we explore the possibility of creating photo-induced birefringent phase grating without surface relief. Independently of their applications for liquid crystal alignment, the nanoscale resolution and light-induced tunability of the optical properties of such layers will make them attractive, on their own merit, for integration in nanophotonic devices to enhance their functionality.

We produced thin films of various PAADs using spin coating methods and measured the thickness and absorption of the films using a stylus profilometer and an optical spectrophotometer, respectively. We combined this information with spectroscopic ellipsometry to estimate their complex refractive index and identified the minimum film thickness required to ensure good optical quality, uniformity and significant photo-induced changes. Photo-induced changes in PAAD films were investigated using an interferometric setup to record gratings and monitor the diffraction efficiency as a function of the recording time and the polarizations of the recording and probe beams. Finally, we used atomic force microscopy to investigate the surface topography of these gratings for any evidence of surface relief.

This paper is structured as follows. Section 2 is devoted to the description of the methodology, in particular different film fabrication and characterization techniques. Section 3 presents the experimental measurements of the physical and optical parameters of the films as well as of their photo-induced changes. Section 4 analyses the results. The conclusions end the paper by highlighting the most important findings and discuss plans for future work.

2. Methodology

The azo dyes used in this study are based on azo-coupling of the diazonium salt of benzidinedisulfonic acid with the derivatives of phenol having different numbers and positions of pendants such as -alkyl and -cyano groups at the phenol ring. Three different versions of PAAD complex dyes were investigated, namely PAAD 22D, 22N and 22E. PAAD are proprietary materials (BEAM Co. Orlando, FL) and the three variations are based on the same chemical composition. They were developed with the aim of shifting the absorption band away from the ultraviolet and into the visible region of the spectrum (towards 532 nm), while maintaining their stability and uniformity. In earlier works, several versions of PAAD-27, 22 and 72 [25], [26] were studied for their contact angle and photoalignment properties with liquid crystals. As presented in Tab. 2, the three samples we have used show some differences in the wavelengths of their absorption peaks. They also have different wetting properties on glass and ITO glass substrates, which influence the uniformity and thickness of the films.

Thin films of PAAD dyes were fabricated by dissolving the dye powder in methanol at a concentration of 1% g/ml and then sonicating for 5 minutes, until a clear solution was obtained. Thin films were deposited on indium tin oxide (ITO) covered glass substrate by spin coating. To obtain uniform films, a set of different speeds, 1000, 2000, 3000, and 4000 revolutions per minute (RPM), of the spin-coater were tested. After deposition, the films were annealed on a hot plate for 10 minutes at 90 °C. In our experiments we used 1 mm thick glass substrates coated with a 30 nm ITO layer typically used in the fabrication of liquid crystal cells. The choice of an ITO/glass substrate was due to the observation that a uniform, smooth film could be achieved by the spin coating on this substrate, most likely due to the good wetting properties of the ITO [27] to the dye solution. Single crystal silicon was also investigated as a substrate due to its high refractive index, as compared to glass and azo dyes, which could potentially lead to more accurate ellipsometric measurements. However, we found it difficult to obtain uniform thin films on silicon due to its poor wetting properties [27].

The complex refractive indices of the PAAD films were determined using ellipsometry [28, 29] (J. A. Woollam M2000DI and a Horiba Scientific UVISEL HR460 ellipsometer). We measured the polarization state of the light reflected by coated and uncoated substrates. The measured behavior was fitted with models of the optical properties of the PAAD layer. In order to independently check the fitting procedure, we separately measured the thickness and the optical absorption of the films.

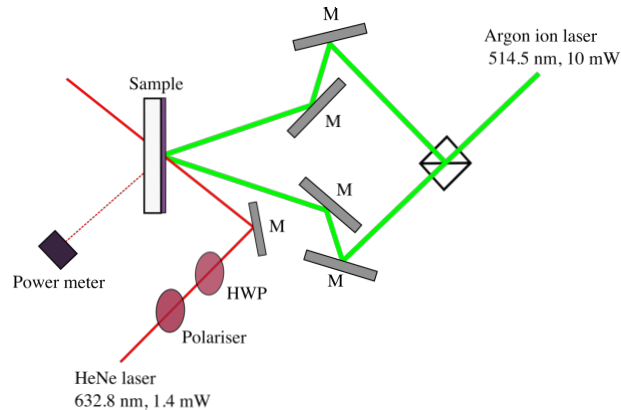


Fig. 2. A 514.5 nm Ar^+ laser was used for writing the gratings and a He-Ne laser at 632.8 nm was used for monitoring the diffraction efficiency (η). The laser powers are measured at the surface of the sample.

The thickness (and its uniformity across the surface) was determined by surface profilometry (KLA Tencor P-16 Stylus Profiler) in different locations of the same sample. Absorbance was determined using a UV/VIS/NIR JASCO spectrometer by comparing measurements before and after spin coating.

The photo-induced response (refractive index change) of thin PAAD films was investigated by monitoring the diffraction from phase gratings recorded in the films by interferometric illumination. A periodic intensity pattern was created by the interference of two mutually coherent Ar^+ laser beams at 514.5 nm, a wavelength strongly absorbed by the PAAD films, using a Michelson interferometric arrangement [30], as shown in Fig. 2.

The angle between the recording beams was 30° , corresponding to a grating period of $1 \mu\text{m}$. The measurements presented below are for the case of the pump beams having linear polarization and perpendicular to the plane of incidence, which creates an interference pattern with the maximal contrast of the fringes. For consistency, we also explored the other configuration and recorded a grating with the recording beams being polarized parallel to the plane of incidence. The total recording laser power was 10 mW. The formation of photo-induced grating was probed in real time by a HeNe laser beam (at 632.8 nm) with a power of 1.4 mW, and incident at the corresponding Bragg angle for this wavelength, which is 18.5° . The choice of a HeNe laser as a probe is due to the low absorption of the PAAD films at 632.8 nm ensuring that the probe light will have a negligible effect on the photo-induced grating. The diffraction efficiency, η , was measured for two polarizations of the probe beam, parallel (η_{\parallel}) and perpendicular (η_{\perp}) to the plane of incidence. It was calculated by dividing the power of the first order diffracted beam by the power of the incident beam. The measurement of the diffracted beam power was performed after the grating recording had reached saturation and with the recording beams turned off. The interference patterns that were recorded in the film erased by uniform illumination of the recording area using just one of the recording beams at 5 mW power.

Finally, AFM maps were acquired [31] by a MultiMode Nanoscope V AFM (Veeco Metrology Group) in contact mode using commercial Al coated Si tips (Budget sensors, Tap300Al-G) with $125 \mu\text{m}$ long cantilevers, resonant frequency of 300 kHz and force constant of 40 N/m.

Table 1. Average thicknesses of films made of the three different materials (22D, 22N and 22E), spin coated at different speeds measured using a profilometer. The errors were calculated by taking the standard deviation of measurements at different locations across each sample.

Sample	1000 RPM	2000 RPM	3000 RPM	4000 RPM
22D	150 ± 50 nm	35 ± 15 nm	20 ± 10 nm	15 ± 10 nm
22N	90 ± 10 nm	70 ± 10 nm	25 ± 5 nm	15 ± 5 nm
22E	65 ± 20 nm	35 ± 20 nm	45 ± 20 nm	45 ± 20 nm

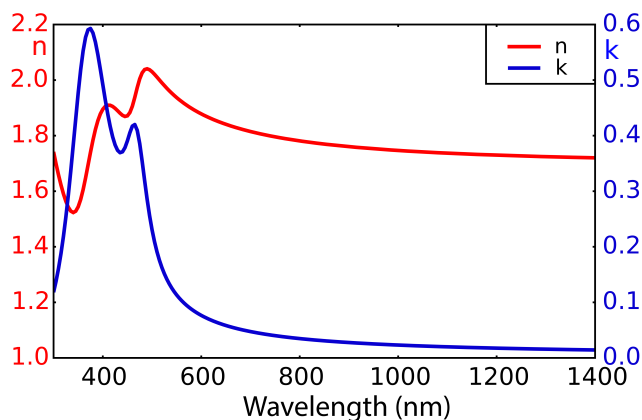


Fig. 3. Complex refractive index, $n + ik$, of 22D on ITO/glass substrate determined by ellipsometry. The same absorption peaks were observed with absorption spectroscopy at 375 nm and 460 nm.

3. Experimental results

The thickness of different PAAD layers and their uniformity depending on the speed of spin-coating are presented in Tab. 1. The films of 22N and 22D dyes appeared to produce more uniform films and their thickness variation across the film and surface roughness was lower in comparison with 22E. The AFM depth measurements have an error of approximately 1 nm, much smaller than the surface roughness of the material. Therefore, the error bars reported in Tab. 1 are a measure of the film non-uniformity rather than the measurement resolution.

Surface profilometry revealed thickness variations that depended on the material and the spin coating rotation speed. As a rule of thumb, increasing the rotation speed made the samples thinner and more uniform. At high spin speed, a layer thickness down to 15-20 nm was easily achievable for the 22D and 22N compounds, with small deviations across the sample. The 22E films were more rough and not entirely uniform even at 3000 and 4000 RPM. The measured surface roughness is included as error in Tab. 1.

In the remaining part of this study, we used the thinnest and most uniform PAAD samples produced at 4000 RPM. For these samples, the profilometer estimates of the layer thickness were independently verified by the ellipsometry measurements.

Figure 3 shows the result of the complex refractive index measurements of the PAAD 22D films in the spectral range from 300 to 1400 nm determined by ellipsometry. The ellipsometry data in the spectral region between 800 - 1400 nm were fitted using a Cauchy model [32] in order to evaluate the thicknesses of the thin films. The complex refractive index $n + ik$ of the PAAD films were evaluated using Lorentz oscillator [33] and B-spline [32] models, which have been widely applied for the calculation of refractive indices. The B-spline model was applied

for all three samples. For the 22D, the results were also confirmed with the double Lorentz oscillator model in the whole spectral region; the obtained complex refractive index is shown in Fig. 3. This model takes an advantage of the two clear absorption peaks of PAADs, that were also independently confirmed by the absorption measurements. For example, as shown in Fig. 3, for modeling of the complex refractive index of 22D, the frequency values of the two Lorentz oscillator resonances were set to 3.3 eV (375 nm) and 2.7 eV (460 nm).

Table 2. Middle column - Absorption peaks of the three different PAAD materials as determined by spectrometric measurements. Right column - Average refractive index in the range 800 to 1400 nm determined using ellipsometry.

Sample	Absorption peaks ± 5 (nm)	Average refractive index
22D	375 & 460	1.8 \pm 0.1
22N	380 & 470	1.6 \pm 0.1
22E	375 & 440	1.8 \pm 0.1

As shown in Fig. 3, the real part of the refractive index of PAAD 22D, n , increases in the 400 to 500 nm range, where there are also the absorption resonances, and then decreases to an approximately constant value of 1.7-1.8 from 700 nm onward. We can use the imaginary part of the refractive index, k , to estimate the wavelength dependent absorption coefficient, $\alpha = 4\pi k/\lambda$, of the material. The PAAD 22D absorption coefficient reached $200 \times 10^3 \text{ cm}^{-1}$ at peak absorption, gradually reducing to 60 and then to 20 and $12 \times 10^3 \text{ cm}^{-1}$ at 500, 600 and 700 nm, respectively. A similar dependence was observed in the other PAAD materials investigated, namely 22N and 22E. Their average refractive index was smaller than for 22D, but strong absorption peaks were also present near 400 nm. The average refractive index for all the films in the wavelength range between 600 nm and 1200 nm is presented in Tab. 2. As shown in Tab. 2, PAAD has a relatively high refractive index in this wavelength range, in particular for 22D and 22N, where its values reach 1.8.

The average refractive indices have been calculated using a range of ellipsometric fits that were then verified using our profilometry and absorption measurements. The refractive index of azobenzene dyes, as determined by other groups [34], was $n_{azo}=1.77$, a value that agrees well with our measurements.

As discussed in the introduction, the light induced changes in azobenzene can be exploited to record polarization patterns. We used this effect to write diffraction phase gratings, using the set-up shown in Fig. 2.

The recording dynamic of the photo-induced diffraction gratings have been measured using the experimental arrangement that was described earlier. The temporal response of PAAD 22D, 22E, and 22N films is shown in Fig. 4. The dynamics of the 22N film is considerably slower than the other two dyes. We have fitted the curves in Fig. 4 using exponentials: the time constants are approximately 5, 4 and 120 s for PAAD 22D, 22E and 22N respectively.

Table 3. Diffraction efficiency of three different PAAD dyes for linear polarization of the probe beam perpendicular (third column) or parallel (fourth column) to the plane of incidence. The second column lists the film thickness for the samples used for these measurements, while the last two columns list the birefringence parameter estimated using equation (1).

Sample	Thickness [nm]	η_{\perp}	η_{\parallel}	Δn_{\perp}	Δn_{\parallel}
22D	20 \pm 5	3×10^{-6}	6.1×10^{-8}	1.7×10^{-2}	2.4×10^{-3}
22N	35 \pm 5	3×10^{-5}	2.1×10^{-7}	3.0×10^{-2}	2.5×10^{-3}
22E	35 \pm 15	1×10^{-6}	6.1×10^{-8}	5.5×10^{-3}	1.3×10^{-3}

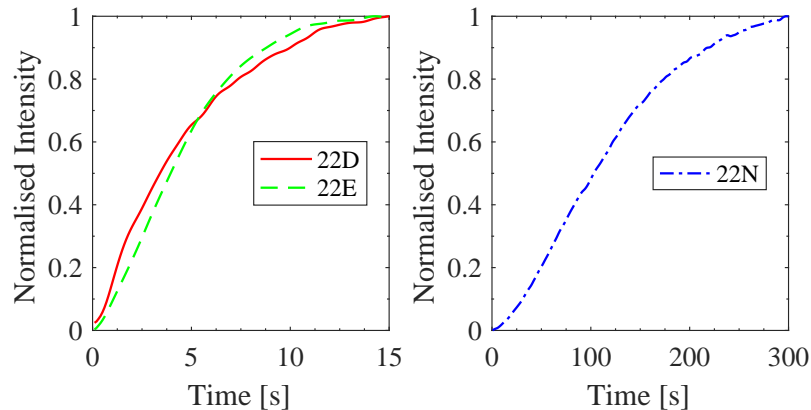


Fig. 4. Normalized intensity of the first diffracted order as a function of time for 22D and 22E (left), and 22N (right).

After the grating was recorded, we measured the dependence of the diffraction efficiency, η , on the relative polarization of the probe to the pump beams. For these measurements we used samples with film thickness varying from 20 to 70 nm. The saturated values of the diffraction efficiencies that correspond to different polarizations of the probe beam are presented in Tab. 3 for the thinnest uniform samples that we were able to achieve. The saturated values of the diffraction efficiencies that correspond to different polarizations of the probe beam are also presented in this table. The grating in the 22N film showed the highest diffraction efficiency with η_{22N} estimated as 3×10^{-5} , while in samples 22D and 22E, the diffraction efficiency was an order of magnitude lower (approximately 10^{-6}). Moreover, the diffraction efficiency, rather unexpectedly, depends strongly of the relative polarization of the pump to the probe beams. The ratio between diffraction efficiencies in the two polarization states varies from 16 in 22E to above 100 in 22N sample. In all cases the highest value of the diffraction efficiency was observed when the polarization of the probe beam matched the polarization of the recording beams. We also repeated the same measurements for gratings recorded with beams polarized parallel to the plane of incidence. In this case, the highest diffraction was again observed when the probe beam had the same polarization as the recording beams, and the ratio between diffraction efficiencies for two orthogonal polarizations of the probe beam was consistent with the previous case.

Such high values of diffraction efficiency from 20 nm thin films indicate that light undergoes a strong modulation while traversing the laser-recorded diffraction grating in the PAAD layer. In order to determine the origin of the modulation, namely surface relief and/or refractive index modulation, AFM imaging of the surfaces was carried out. This failed to show any periodic surface relief pattern. Moreover, the lack of surface relief pattern justifies the observed diffraction efficiency dependence on the polarization of the recording beams: the manner of the surface relief grating should not change simply by rotating the polarization of the recording beams. The absence of surface relief in the thin films considered here is in contrast with reports on thicker layers [16]. It is, however, consistent with the observation that linearly polarized light is less effective at producing surface relief in 150 nm-thick layers [17]. A direct comparison between our work and this last publication is not possible as the polarization of the pump beams used in the two cases is different. In [17], the pump beams had either co- and contra-circular polarization, or linear orthogonal polarization, while in our experiments the pump beams were always co-polarized. In summary, it is therefore likely that for very thin films, as investigated in our study, the lack of polymer structure and stronger influence of the surface impedes the formation of relief gratings.

The assumption that illumination creates a refractive index grating can, in principle, explain this polarization sensitivity: the polarized recording beam induces birefringence in PAAD materials, causing different refractive index changes in the directions parallel or perpendicular to its polarization. However, this interpretation is not straightforward, as we discuss in the next section.

4. Discussion

Following the exclusion of a surface relief grating contributing to the measured diffraction efficiency, we are forced to associate the observed diffraction purely to a modulation of the refractive index. The diffraction properties of PAAD layers are normally modeled using Jones matrices [13, 16, 17]. However, the linear polarization of the recording beams that we have used produced a very simple polarization grating in which the illuminated regions now have an optical axis that is perpendicular to the pump beam polarization, i.e. in the plane of incidence, while the dark regions remain isotropic. In this case, the Jones matrices simplify considerably and we can consider the PAAD film as an isotropic grating with a refractive index modulation that depends on the polarization of the incident probe beam. Furthermore, as the film is thin with respect to the recording wavelength we are firmly in the Raman-Nath regime [35, 36], and the diffraction efficiency is given by [37]

$$\eta = J_1^2 \left(\frac{2\pi\Delta n d}{\lambda \cos(\theta)} \right) \implies \Delta n \simeq \frac{\lambda \cos(\theta)}{\pi d} \sqrt{\eta}. \quad (1)$$

Here J_1 is the Bessel function of the first kind of order 1, Δn is the amplitude of the refractive index modulation, λ the probe wavelength in vacuum, d the film thickness and θ the probe angle of incidence. The approximation on the right hand side of equation (1) is excellent for our values of η .

The two rightmost columns in Tab. 3 list the amplitudes of the refractive index modulations seen by a probe beam polarized perpendicular (Δn_{\perp}) or parallel (Δn_{\parallel}) to the plane of incidence required to produce the measured diffraction efficiencies. The largest of these modulations is for a probe beam polarized in the direction perpendicular to the plane of incidence (matching the polarization of the recording beams). What is most significant in these data is that the ratio $\Delta n_{\perp}/\Delta n_{\parallel}$ is 4, 7 and 12 in 22E, 22D and 22N PAAD films, respectively. This large difference in refractive index is not explainable using standard molecular reorientation models for PAAD layers [7].

In these models, the molecules are assumed to be rod-shaped. When in the isotropic phase, there is no collective preferred direction among the PAAD molecules. Hence the film is optically isotropic and has refractive index n_I . When there is a collective orientation present, the film acquires an optical axis parallel to the molecules average orientation and has associated ordinary and extraordinary refractive indices, n_o and n_e , respectively, proportional to the degree of order of the molecular axes. As a result, the film now acts as a birefringent medium in the illuminated regions, with the optical axis laying in the direction perpendicular to the pump beam polarization.

The refractive index modulation in the grating region is obtained by assuming that the dark regions are in the isotropic phase and that the illuminated regions are partially oriented. If we assume that the film constrains the molecules to lie in its plane, then the isotropic refractive index is $n_I^{(2D)} = (n_o + n_e)/2$. The two polarizations of a probe beam coming at a normal incidence observe the same refractive index amplitude modulation $\Delta n_{\parallel}^{(2D)} = \Delta n_{\perp}^{(2D)} = (n_o - n_e)/2$ and, hence, the same diffraction efficiency. For the tilted incidence, however, a probe beam polarized in the plane of incidence experiences an effective refractive index in the illuminated region, which depends on the angle of incidence:

$$n_{\text{eff}}(\theta) = \frac{n_o n_e}{\sqrt{n_o^2 \cos^2(\theta) + n_e^2 \sin^2(\theta)}}. \quad (2)$$

Therefore, in general $\Delta n_{\parallel}^{(2D)}$ is a function of θ , $\Delta n_{\parallel}^{(2D)}(\theta) = n_{\text{eff}}(\theta) - n_I^{(2D)}$. In principle it is possible, by a careful choice of the angle of incidence θ , to make $\Delta n_{\parallel}^{(2D)}$ as small as we wish. However, at the angle of incidence used in the experiment, $\theta = 18.5^\circ$, n_e and n_o would have to be at least $1.5n_I^{(2D)}$ and $0.5n_I^{(2D)}$ respectively, in order to produce the experimental $\Delta n_{\perp}/\Delta n_{\parallel}$ ratios. These values are far too large to be acceptable.

Alternatively, we can assume that the film is sufficiently “fluid” that the PAAD molecules can equally reorient in three dimensions. In this case, the isotropic refractive index is $n_I^{(3D)} = (2n_o + n_e)/3$. The illumination with the pump beam polarized perpendicular to the plane of incidence decreases the population of molecules oriented in this direction, introducing a short optical axis with the refractive index of n_o . The molecules, though, are still free to orient in any direction with equal distribution in the plane of incidence. The probe beam polarized parallel to the plane of incidence would therefore experience an effective refractive index of $(n_o + n_e)/2$, which does not depend on the angle of incidence. The amplitudes of refractive index modulation are then given by

$$\begin{aligned}\Delta n_{\parallel}^{(3D)} &= \frac{n_o + n_e}{2} - n_I^{(3D)} = \frac{n_e - n_o}{6}, \\ \Delta n_{\perp}^{(3D)} &= n_I^{(3D)} - n_o = \frac{n_e - n_o}{3}.\end{aligned}\quad (3)$$

The ratio between the two modulations is 2, independently of the absolute birefringence of the PAAD molecule assembly. Whereas the 3D model yields the correct trend, the ratio between $\Delta n_{\perp}^{(3D)}/\Delta n_{\parallel}^{(3D)}$ is much smaller than experimentally measured values.

This analysis suggests that the origin of the refractive index modulation cannot be fully attributed to a molecular reorientation effect. More experiments are needed to understand this remarkable observation and ascertain its stability and dependence of the film parameters, furthermore, the interaction of the PAAD films with the substrate surface has to be studied further. It is possible, for example, that the thinness of the layer modifies the diffusion dynamics in the Angular Hole Burning model [7] in a polarization dependent manner.

5. Conclusions

In this work three different azobenzene complex dye films, PAAD 22D, 22E and 22N, were characterized for their main physical and optical properties. Uniform films with thickness from 150 nm down to 15 nm were fabricated on ITO coated glass substrates by using different spin coating speeds. The complex refractive indices of the PAADs were measured using ellipsometry and absorption spectroscopy. Furthermore, the profilometry measurements were also carried out to cross check and confirm the validity of the ellipsometric results. The films had relatively high refractive index, namely from 1.6 to 1.8. It was shown that even thin films, with thickness below 35 nm, lead to considerable diffraction efficiency with gratings formed through the refractive index change rather than surface relief. PAAD films show considerable photo-sensitivity, in spite of limited thickness, and can be attractive for functionalizing surfaces and structures. Previous reports on thicker films of similar azo-based materials associated diffraction mostly due to surface relief rather than a refractive index change. Most importantly we have also shown that the photo-induced refractive index change in PAADs is anisotropic with largest refractive index modulation in the direction parallel to the polarization of the writing beams. This phenomenon cannot be attributed to a molecular reorientation effect. This intriguing mechanism of interaction of thin PAAD films with light will be studied further, in particular by considering the interaction with the substrate surface and its role in the formation of the gratings.

Funding

Defence Science and Technology Laboratory & Direction générale de l'armement (DSTL-DGA) joint PhD grants (DSTLX-100074647, DSTLX-1000105958); UK Engineering and Physical Research Council (EPSRC) (EP/J007676/1).

Acknowledgments

We are grateful to Dr A. Priimagi, Prof. Marina Saphiannikova-Grenzer for their helpful comments and insights and Prof. Themis Prodromakis for the AFM measurements.

All data supporting this study are openly available from the University of Southampton repository at <http://doi.org/10.5258/SOTON/D0364>.